Time-Resolved Laser-Induced Desorption Spectroscopy (LIDS) for Quantified In-Situ Hydrogen Isotope Retention Measurement and Removal from Plasma Facing Materials

J.H. Yu, M.J. Baldwin, M.J Simmonds, and A. Založnik

Abstract

A laboratory scale laser induced thermal desorption spectroscopy system is developed and tested on tungsten-deuterium and titanium-deuterium codeposits, and its feasibility as a hydrogenic inventory measurement diagnostic is demonstrated over a range of retention values from $5x10^{19}$ m^{-2} to $7x10^{23}$ m^{-2} for absorbed laser power densities as low as 8 MWm^{-2}. Codeposit layer samples are grown by magnetron sputtering and immersed in a weak argon rf plasma. A 1 kW fiber laser (λ = 1100 nm) heats the samples up to a peak surface temperature ranging from 900 to 1500 K using pulse widths of 0.05 to 1 s. Spectral line emission from Balmer series Dα and Hα from thermally-desorbed deuterium and hydrogen, as well as line emission from argon, are monitored as a function of time using an optical spectrometer with maximum temporal resolution of 1 ms. To correct for wall recycling and pumping speed, and to accurately measure the time evolution of the laser-induced thermal desorption, the raw Dα signal is deconvolved with the system response function, which is obtained by injecting a short burst of D_2 to approximate an impulse. Calibration is done with a standard D_2 leak, and LIDS deuterium retention values are found to be in good agreement with companion measurements made using conventional temperature programmed desorption (TPD) on samples from the same codeposit batch.

I. Introduction

In nuclear fusion devices, the interaction of the edge plasma with the plasma facing components (PFCs) leads to various effects. Such effects include surface erosion by sputtering, layer growth from the re-deposition of sputtered PFC material, and trapping of deuterium (D) and tritium (T) fuel species within the PFC material or the deposited layers (commonly referred to as codeposits). For the nuclear fusion endeavour, fuel trapping, or rather the loss of T from the fuel cycle, is problematic as T management practice must satisfy low in-vessel limits to meet the requirements of both nuclear safety licensing and tritium breeding [1]. As a consequence, strategies are required for T inventory assessment and control in fusion reactor PFCs, and diagnostic capabilities that can measure and/or remove T from plasma-wetted surfaces and material deposition areas are currently high priority research tasks in ongoing fusion research [2].

There are few reliable methods for quantifying hydrogen (H) isotopes in material surfaces. Nuclear reaction analysis (NRA) is a widely used technique for such measurements, utilizing high energy projectile ions to form detectable nuclear products from subsurface target species such as H, but NRA is not suitable as an in-vessel fusion diagnostic due to the need for a typically large accelerator to produce the high energy ion beam. Recently, there has been a renewed interest in laser-based methods [3-5] combined with optical spectroscopy to locally measure and remove hydrogenic species from materials in-situ, including laser induced breakdown spectroscopy (LIBS) [6-13], laser induced ablation spectroscopy (LIAS) [14, 15], and laser induced desorption spectroscopy (LIDS) [16-18]. With LIBS, high peak power densities achievable with short pulse lasers (fs to tens of ns) create a laser-induced plasma

from ablated material, which is characterized spectroscopically. In contrast, LIAS and LIDS employ an external plasma to excite laser-desorbed material for spectroscopic identification and quantification. Lasers with intensity below the ablation threshold, such as those used in LIDS, release trapped hydrogenic species from materials via thermal desorption without destruction of the material surface.

In fusion applications, laser-induced release of gas from stainless steel was first investigated by Schwirzke [19] using measurements of pressure rise to infer released gas quantities, but no identification of the released gas was made. Further development of laser desorption [20, 21] has progressed using various detection schemes to measure desorbed species, including a time-of-flight mass spectrometer [22], a quadrupole mass spectrometer (QMS) [23], a QMS in conjunction with NRA [24], and temperature programmed desorption (TPD) before and after laser heating [25]. Pioneering LIDS work at the TEXTOR tokamak used the edge plasma to excite laser-desorbed deuterium and a CCD camera and interference filter to detect Dα optical emission [4, 16-18]. In that work, the laser pulse width was 1 to 10 ms, which provided spatial control of heat deposition by limiting lateral heat diffusion.

In this article, we explore LIDS as a diagnostic system with the potential for targeted, in-situ, hydrogen isotope measurement in and removal from PFC surfaces, and present a new analysis method for LIDS data. The experimental setup for time-resolved LIDS is outlined and we describe a deconvolution analysis technique which corrects for the repeated interchange of hydrogenic species between the vessel wall and the plasma, a process known as wall recycling [26]. Deconvolution provides an accurate measurement of the time-evolution of desorption, which is necessary if comparing LIDS data with hydrogen diffusion reaction models. The use of deconvolution is not limited to LIDS but can also be applied to any detection scheme where recycling, or other time-dependent system effects, alter the detected signal.

The LIDS system described here differs from other LIDS measurements in one or more of the following ways: 1) the spectral resolution of the spectrometer allows separation of Dα from nearby spectral lines using spectral fitting, 2) the temporal resolution of the spectrometer is sufficiently high relative to the laser pulse width to allow for a time-resolved measurement of desorption, 3) a calibrated D_2 leak located near the laser-irradiated area provides quantitative measurements of desorbed deuterium, eliminating the need for precise knowledge of spatially-dependent plasma parameters required for the S/XB technique, and eliminating the need for the optical field of view to cover the entire region of Dα emission, 4) the system response function is measured experimentally using an impulsive burst of D_2 gas injection, and 5) numerical deconvolution of the measured signal with the system response function provides a correction for system-dependent time effects such as wall recycling and finite pumping speed.

II. Codeposit Preparation

Both titanium-deuterium (Ti-D) and tungsten-deuterium (W-D) codeposit layers were created for LIDS experiments in the present work. The Ti-D codeposits were used to provide good signal during LIDS by taking advantage of the high storage capacity of titanium thin films, leading to a large hydrogenic release for optical detection and measurement. The second case of W-D codeposits demonstrated the technique on a fusion relevant material, and showed the technique can be used on material with significantly less D inventory than that in Ti.

Identical Ti-D codeposit samples were prepared by magnetron sputtering of Ti targets with an argon sputtering plasma, using Ar fill pressure of 5 mTorr while simultaneously injecting D_2 with a fill pressure of 2.5 mTorr. Two batches of Ti-D codeposits were created using 25 mm diameter and 2 mm thick nickel discs as substrates, with codeposit layer thicknesses of 1.3 and 4.0 μm, both with surface temperature <500 K during deposition. A batch of identical W-D codeposits were also prepared by magnetron sputtering in an argon-deuterium mixture with 0.5 mTorr of Ar fill pressure and 9.5 mTorr of D_2, and surface temperature <350 K. The substrates for W-D layers were chosen to be 6 mm diameter W discs with thickness of 1.5 mm. The reason for using smaller substrates was to laser-heat the entire sample surface during LIDS, removing uncertainty about the area of desorption. Three batches of W-D codeposits were created with layer thickness ranging from 1.2 to 4.6 μm.

One sample from each batch was analyzed for D content using TPD, in which samples were separately heated in the TPD oven at a rate of 0.3 K/s from 300 to 1200 K, while monitoring the released D_2, HD, and H_2 with a residual gas analyzer which was calibrated with a known D_2 leak rate. A background subtraction method [25] was used to eliminate contribution to the HD and D_2 signals arising from water vapor in the TPD system, and the sensitivity for HD was assumed to be the same as that for D_2.

III. Laser, Plasma, and Spectrometer

The codeposited samples were immersed one at a time in an inductively coupled rf (13.56 MHz) plasma in argon, with steady-state rf power of 1000, 1500, and 2000 W used for each of the different samples. The plasma density and electron temperature were measured with a Langmuir probe and were 5 - 9x10^{16} m^{-3} and 3 – 4 eV, respectively. A fiber laser (Coherent Highlight 1000FL) with wavelength of 1100 nm, rectangular temporal shape, and approximately Gaussian spatial profile was used to heat the samples. Samples were air-cooled from the backside and the sample temperature was below 320 K immediately before laser irradiation. A 2-color pyrometer monitored the sample surface temperature during laser induced desorption (LID), and a spectrometer (Avantes AvaSpec ULS2048) was used to measure Balmer series Dα and Hα emission, as well as Ar I line emission. Figure 1 shows the experimental setup of the fiber laser, plasma chamber, spectrometer, pyrometer, and calibrated D_2 source (Laco Technologies) providing a flow rate of 5.2 x 10^{16} D/s. RF power was coupled to the plasma from a helicon antennae encircling a quartz bell jar, located approximately 30 cm above the sample. Plasma density decreased as a function of axial distance (z) from the antennae due to the fact that the ionization source was localized near the antennae. This decrease in plasma density is shown in Figure 2, which shows measurements of electron density, n_e, and electron temperature, T_e, both measured with a Langmuir probe, as well as measurements of Ar I and Ar II spectral line intensity, converted to spectral radiance using a calibrated light source (Optronic Laboratories 455-12 integrating sphere). The argon line emission has a similar z-dependence as electron density, which is expected for relatively homogeneous T_e as in the rf plasma. Due to the higher electron density near the bell jar and thus larger spectroscopic signal-to-noise, the spectrometer was aimed in the upward direction at an angle of 30 degrees with respect to horizontal during LIDS measurements.

In the case of Ti-D codeposits, the laser spot size ($1/e^2$ width) on the samples was ~3 mm as measured by laser burn paper, and the absorbed laser power densities ranged from 20 to 100 MWm^{-2}. For these samples, the laser spot size was smaller than the sample size of 25 mm diameter. Lateral heat

diffusion during the laser pulse was a source of uncertainty on the exact desorbed surface area, which depended on both the laser intensity and the pulse width. To avoid this uncertainty, smaller sample sizes of 6 mm diameter were used in the case of W-D codeposits, and the laser spot size was increased to 10 mm in order to cover the entire sample and to provide a relatively uniform irradiation across the sample. From the center of the sample to the edge, the laser intensity variation was approximately 25% as measured with a camera imaging diffusely reflected laser light. Temperature-independent reflectivities of 0.56 [27] and 0.63 [27, 28] were assumed for Ti and W, respectively, in the present paper when quoting absorbed power densities.

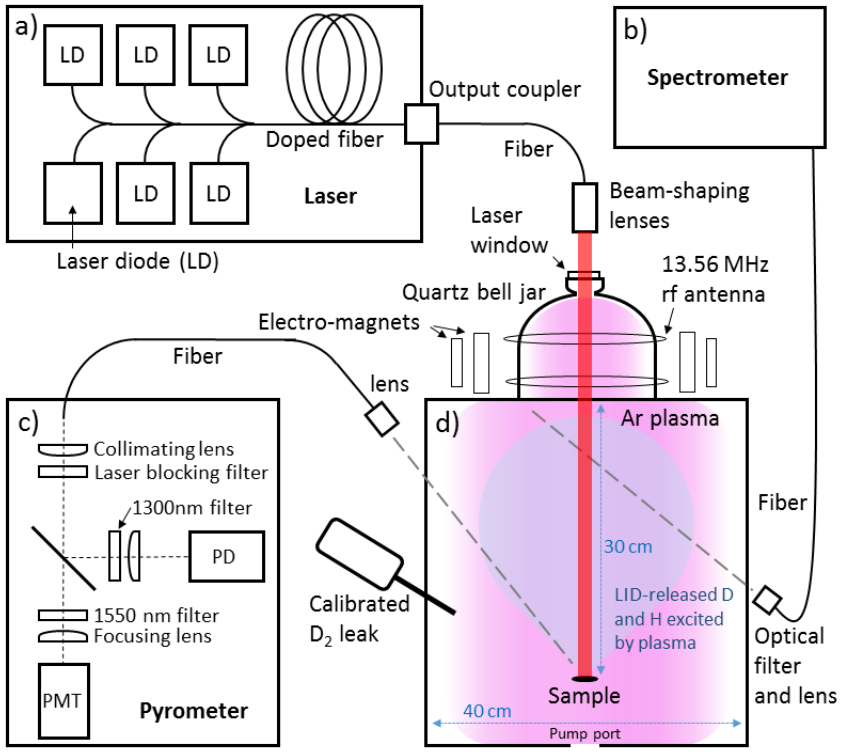

Figure 1 Schematic of experimental setup for LIDS: a) fiber laser, b) spectrometer, c) pyrometer, d) rf plasma chamber with calibrated D_2 leak.

A fast pyrometer built in-house [29] was used to detect thermal emission from the sample surface to determine surface temperature evolution during LIDS. An optical filter that transmitted $\lambda >$ 1200 nm was used to block unwanted laser light. The light was then split using a beamsplitter and passed through interference filters, each with a spectral bandwidth of 100 nm, and a photo-diode (PD) and a photo-multiplier tube (PMT) were used to detect 1300 and 1550 nm radiation, respectively. Additional neutral density filters were used in front of the PMT as needed to avoid saturation. The temporal resolution of the PD depended on the gain and was typically <1 ms, while the PMT had a faster response of ~10 μs. The pyrometer was calibrated using a W strip lamp with known temperature as a function of lamp current. A 2-color method was used to calculate the surface temperature (avoiding the need to know absolute emissivity), which relies on the assumptions that the ratio of the sample emissivities at the two measured wavelengths during the actual measurement was the same as that

during the calibration, and that the ratio of emissivities does not change as a function of surface temperature.

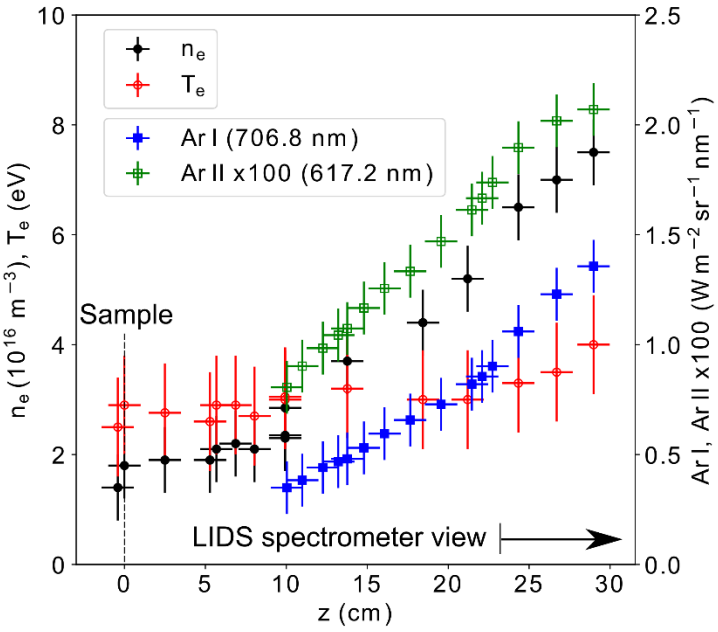

Figure 2 Plasma parameters, ne and Te, and the spectral radiance from line-integrated measurements of Ar I and Ar II spectral lines, measured as a function of height in the rf plasma chamber with rf power of 1500 W and Ar fill pressure of 10.6 mTorr.

IV. Spectroscopy of Desorbed Deuterium

A. Spectral fitting

The Avantes spectrometer resolution of 0.35 nm near the wavelength of hydrogenic alpha emission was not sufficient to distinguish the peaks from Dα (656.10 nm) and Hα (656.28 nm). This meant that sources of H (water vapor is always a contributor) would alter the measured amplitude and shape of the Balmer line observed during the LIDS pulse. The issue was addressed by separating the D and H contributions using a spectral fitting procedure that used experimentally-determined spectra for Dα and Hα separately. We fit the measured Balmer line with a linear superposition of two functions,

$$S(\lambda) = a_D f_D(\lambda) + a_H f_H(\lambda),$$

where S is the modeled spectrum, a_D and a_H are fitting parameters for the amplitudes of Dα and Hα, respectively, and the functions f_D and f_H are the measured spectra when pure D_2 or pure H_2 is injected into the Ar plasma, respectively, normalized to unity amplitude. These functions are the spectrometer response to each species and are fixed during the fitting procedure, that is, the only fitting parameters are a_D and a_H. Note that this method does not rely on choosing an appropriate analytic function for the line shapes because the functions are obtained from actual measurements. In the case of D_2 injection, the Dα signal is orders of magnitude larger than the inherent background Hα signal. Examples of this technique are shown in Figure 2 for two ratios of D/H, displaying excellent agreement between the

model and the data. The fit is performed for each spectral scan, which yields the time evolution of a_D and a_H separately.

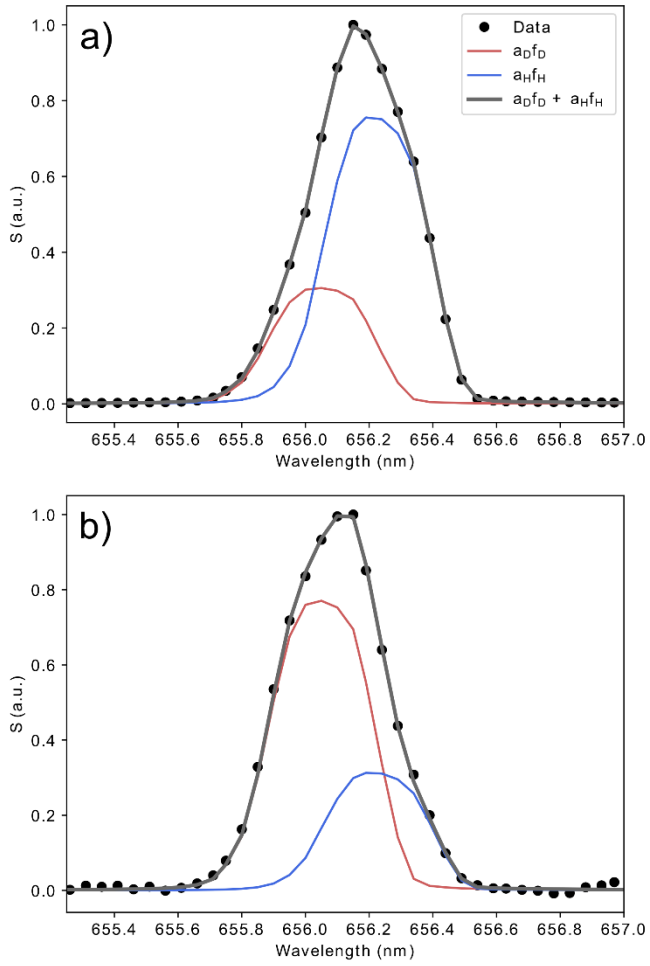

Figure 3 a) Spectral fitting for a_D/a_H = 0.4, b): a_D/a_H = 2.5.

B. Deconvolution and Calibration

Here we present an analysis technique which does not require precise knowledge of plasma parameters or detailed knowledge of particle-wall interactions such as the wall recycling coefficient. Ideally when D_2 is desorbed from the target surface during the LIDS flash, the Dα spectroscopic signal depends on the dissociation efficiency of the D_2 and the excitation cross section for D in the background Ar plasma. Then, use of a calibrated D_2 flow into the same Ar plasma used during the LID event would allow for straightforward conversion of the optical data into D_2 molecular flow from the target surface, as plasma effects and the light collection efficiency are the same in each case. However, one challenge to accurately measuring time-resolved LIDS signals is that a desorbed particle can be counted multiple times due to wall recycling. In addition, the pumping speed of the vacuum system influences the

magnitude and temporal shape of the detected D signal. A deconvolution approach to the data analysis was therefore necessary to address this challenge.

Figure 4 shows the effect of wall recycling and limited pumping speed during calibration with a D_2 leak source. These system effects are evident as an increasing Dα signal (blue curve) with time after a constant D_2 flow from the calibrated leak was switched on (t = 25 s). To correct for these effects, we use the fact that the measured Dα amplitude $a_D(t)$ is a convolution of the true D_2 flow rate f, and a system-dependent response function, g, given by:

$$a_D(t) = c \int_{-\infty}^{\infty} f(\tau) g(t-\tau) d\tau,$$

where c is related to the manufacturer calibration of the constant leak source of D_2. The response function g contains all time-dependent effects of the entire system including wall recycling and pumping speed.

The system response is measured by injecting a quick burst of D_2 gas into the chamber (orange curve in Figure 4) with identical background plasma conditions used during the calibration and LIDS events. The burst approximates an impulse function $\delta(t)$, which allows the response function g to be directly measured using the following expression:

$$\int_{-\infty}^{\infty} \delta(\tau) g(t-\tau) d\tau = g(t),$$

that is, the measured signal from an impulse function is the system response function itself. We inject a sufficient amount of D_2 to give good signal to noise, but not enough to cause perturbation to the background plasma, which we verify by monitoring an Ar I emission line. To reduce noise in the deconvolution, the system response is fit with the sum of three exponential decay functions (black curve).

Once the response function is known, it is then used to obtain the true flow rate (red curve) by deconvolving the measured signal (blue) with the response (black). It is noted that that the numerically deconvolved signal during the calibration flow is reasonably constant as is expected for the D_2 leak. The calibration factor, c, is the proportionality constant between the known calibrated flow rate and the normalized deconvolution. It is clear that failing to take time-dependent system effects into account can lead to misleading measurements (compare blue and red curves), particularly when the time scale of the LIDS event is the same or longer than the timescale of the system response. However, the signal-to-noise ratio of the original signal is typically degraded after deconvolution, which can also lead to artifacts such as the overshoot seen in Figure 4 when the flow is stopped (t = 62 s). We have used inverse filtering (shown here) and Fourier deconvolution algorithms, both with similar results.

The same deconvolution procedure is applied to data obtained during LIDS flash events to obtain the true temporal form of the LID release from targets, and the same calibration factor is applied to convert the deconvolution into particle flow rate. To analyze the LIDS Dα signal, flow calibration and D_2 burst injection (to measure g) should be done shortly after the LIDS measurement while the wall conditions are similar as that during LIDS. We deconvolve the raw Dα LIDS signal with g, and use the same calibration factor obtained from the calibrated flow to determine the actual flow rate of laser-desorbed deuterium. To convert to desorbed flux, the flow rate is divided by the laser-irradiated area, and retention is found by time-integrating the flux up to the end of the heat duration.

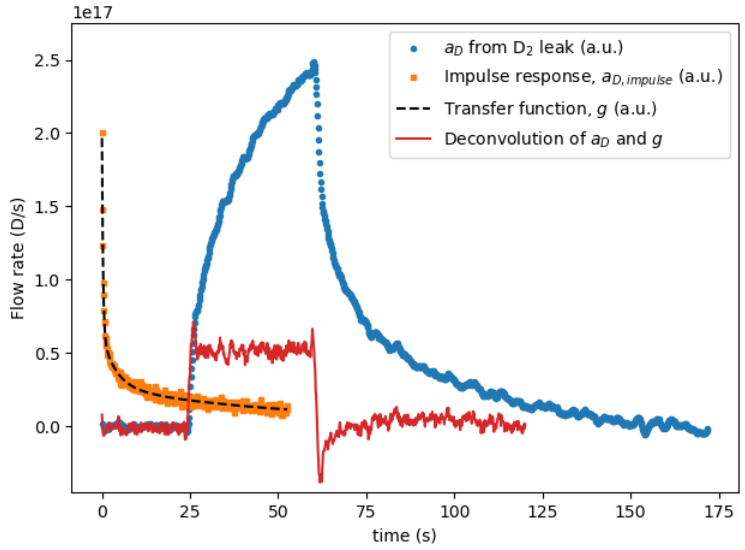

Figure 4 Calibrated, steady, D_2 flow from t = 25 s through t = 62 s. Blue data points are the measured Dα amplitude, which increases due to wall recycling. Transfer function (black) obtained from short pulse of D_2 gas injection (after steady D_2 leak). Deconvolution (red) recovers actual flow rate. Overshoot artifact occurs due to numerical deconvolution when flow is abruptly turned off.

V. Characterization of Time-Resolved LIDS

A. Ti-D codeposits

LIDS datasets for the Ti-D codeposit layer are shown in Figure 5 for an irradiated laser spot of diameter 3.5 mm and pulse width of 0.5 s. The columns in Figure 5 depict three separate laser irradiations of the same sample location. The top row shows the laser waveform, the middle row shows the pyrometer surface temperature measurement, and the bottom row shows the response function of the system (measured after LIDS), the raw Dα emission, and the calibrated deconvolution. In this sequence of laser shots, the laser power was successively increased to obtain full removal of D as demonstrated by the lack of D emission following the second LIDS pulse. The difference in the temporal shape of the raw Dα signal (red) compared to the corrected signal obtained by deconvolution (black) is striking, particularly when a large quantity of D is desorbed as in Figure 5a. The raw Dα signal remains elevated after the laser pulse is finished even though the desorbed flux from the sample is zero. This is due to wall recycling, which effectively increases the pump out time for deuterium released during the laser pulse. In contrast, the deconvolved signal, which is a true signal of desorbed D flux, falls to zero when the sample cools.

When calibrated, the released areal D gives a D retention value of $4.4 \pm 0.9 \times 10^{23}$ m^{-2}. The LIDS measure of D retention is found to agree within experimental error with that obtained on the control sample from the same codeposit batch, measured by conventional TPD. The largest source of uncertainty in determining the flux of D (and thus retention) for the Ti-D codeposits was the area of desorption, which was determined by measuring the diameter of laser-induced discoloration using a confocal microscope.

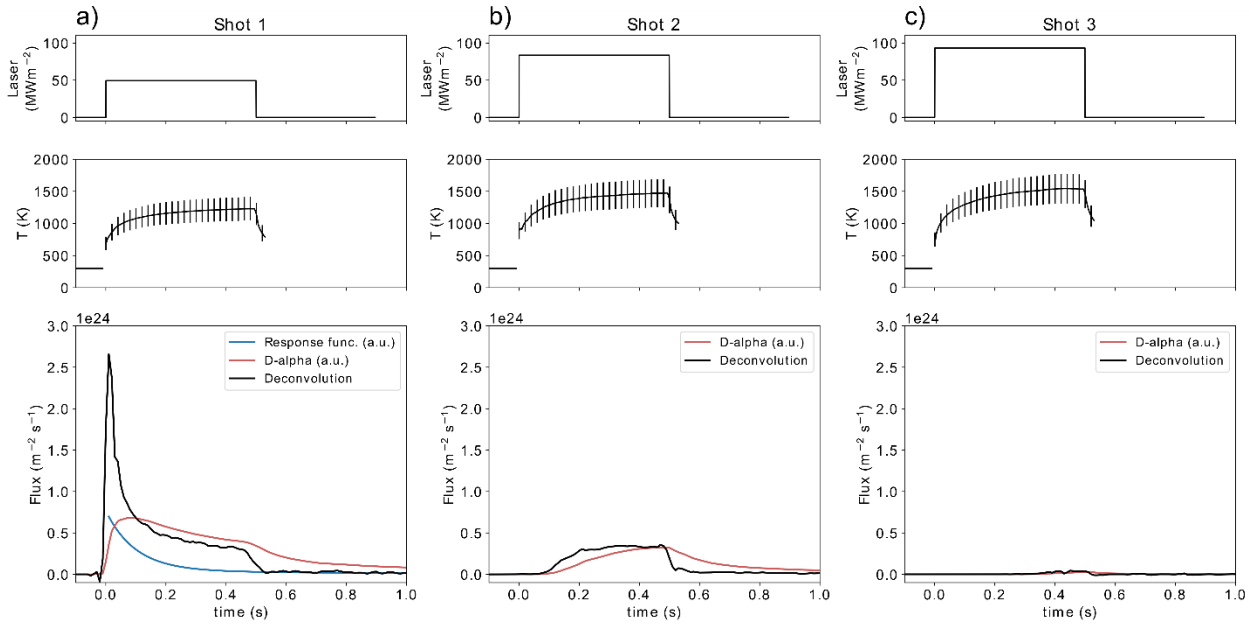

Figure 5 LIDS data for three sequential 0.5 s laser irradiations of a 4 µm Ti-D codeposit layer in the same location, with increasing laser power density from shot-to-shot. Data shown: laser power pulse waveform (top), fast pyrometer surface temperature measurement (middle), and Dα emission (bottom) during LIDS (red), system response function measured offline after LIDS (blue), and the calibrated deconvolution of the response function and Dα (black). The inferred areal D released corresponds to an areal D retention of 4.4 ± 0.9 ×10^{23} m^{-2}, which agrees with a conventional TPD measurement on an identical sample of 3.8 ± 0.6 ×10^{23} m^{-2}.

Figure 6 shows the TPD measurements from a 1 and a 4 µm thick layer; the latter was created in the same codeposit batch as the LIDS sample in Figure 5. TPD reveals a sharp release peak for the 4 µm layer at ~630 K and total areal D retention of 3.8 ± 0.6×10^{23} m^{-2} which corresponds to a D/Ti ratio of approximately 0.6, indicating the layer is predominantly TiD_2. The 1 µm sample has a lower D inventory with the TPD integral yielding a D retention of 1.1 ± 0.3×10^{23} m^{-2}. LIDS was performed on 25 mm diameter samples from this 1 µm layer coating as well, yielding retention values in agreement within error bars with the TPD value. The long tail in temporal shape of the deconvolved LIDS signal in Figure 5 compared to the narrow release peak in the TPD measurement was due to the fact that the temperature was roughly constant in the LIDS data, which gives continual release of D from hydride decomposition [30].

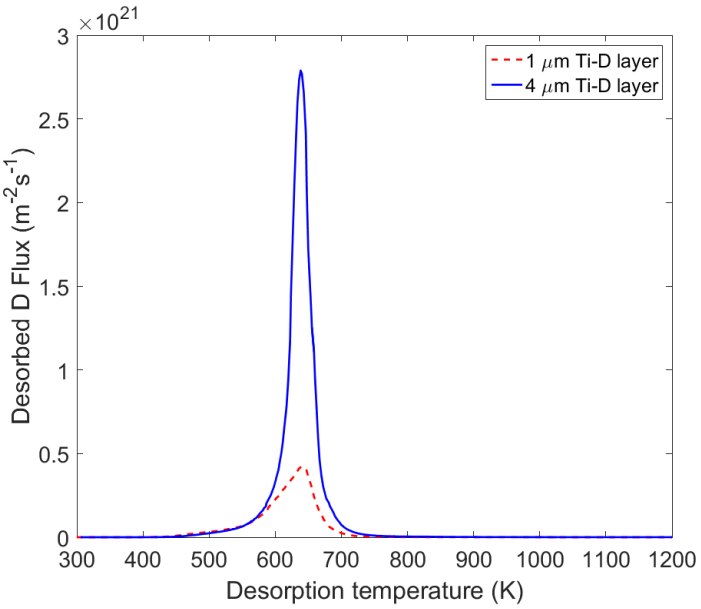

Figure 6 TPD using a temperature ramp rate of 0.3 Ks-1 for two Ti-D codeposits, both created with sample temperature of ~500 K.

B. W-D codeposits

Tungsten will be used as a plasma facing material in future tokamaks such as ITER and DEMO, and here we show LIDS measurements of D retention in W-D codeposits. The trapping and thus desorption physics are different for W-D compared to Ti-D layers; hydrides are formed in Ti-D while in W-D, deuterium is trapped at defects such as dislocations, mono-vacancies, and vacancy clusters, each with its own de-trapping energy [31]. The sharp release peak of D from Ti-D occurs because when the temperature is sufficient to break hydride bonds, D rapidly diffuses to the surface and escapes. In contrast, the broader release peak from W-D is due to a multiple step process of thermally activated de-trapping, diffusion of deuterium through the material, and repeated trapping and de-trapping. A time-resolved measurement of desorbed D, as is presented here, is critical for accurate modeling of this multi-step desorption process.

The quantified LIDS measurement and removal of D from W-D codeposits is demonstrated by comparison of the data presented in Figure 7 and Figure 8. These data represent D release from separate targets from a batch of identical 1.2 µm thick magnetron sputtered W-D codeposit layers prepared on W substrates at 330 K. Figure 7 shows laser-induced thermal release measured by LIDS while Figure 8 gives companion data from conventional TPD. The TPD desorption curve taken at a linear ramp rate of 0.3 Ks-1 up to 1200 K reveals desorptive release at ~500 K and an areal D retention of $1.3\pm0.3 \times 10^{21}$ m^{-2}. Following a single 1 s, 8 MWm^{-2} LIDS flash event, TPD was done on the sample to check how much D remained in the sample (blue curve of Figure 8). The data reveal that approximately 97% of D was desorbed by the laser pulse, with fairly modest power density. In the case of this 1 s laser pulse, no surface damage such as roughening, melting, or ablation is observed. Confocal laser scanning microscope images of the W-D sample before and after laser irradiation show no change, indicating laser parameters which result in peak surface temperatures below the recrystallization temperature, but

above a temperature of ~900 K at which nearly all D escapes, could be used for detritiation with minimal impact on surface quality. However, after high cycle number, thermomechanical properties may be affected due to creep or micro-cracks.

The LIDS data of Figure 7, generated by two successive laser irradiations show similar results to the conventional TPD data of Figure 4, albeit on a more rapid time scale in the case of LIDS. The first 1 s shot in (a) at just under 10 MWm^{-2} leads to fast desorptive release at ~500-700 K in the calibrated de-convoluted Dα signal, and the inferred areal D retention is $1.3\pm0.4 \times 10^{21}$ m^{-2}. The actual Dα signal and system response function are also shown for completeness. A subsequent shot (b) produces no further D release. It is pointed out that for the near full D removal from the target surfaces in each case (TPD and LIDS) the inferred measurements of D areal retention are in excellent agreement, thereby unequivocally demonstrating the viability of calibrated LIDS as a hydrogen isotope inventory measurement and removal diagnostic tool. The LIDS signal-to-noise can be improved significantly in plasma sources with higher densities than those achievable in the rf plasma used here, allowing measurements of lower retention and higher temporal resolution through the use of shorter integration times on the spectrometer.

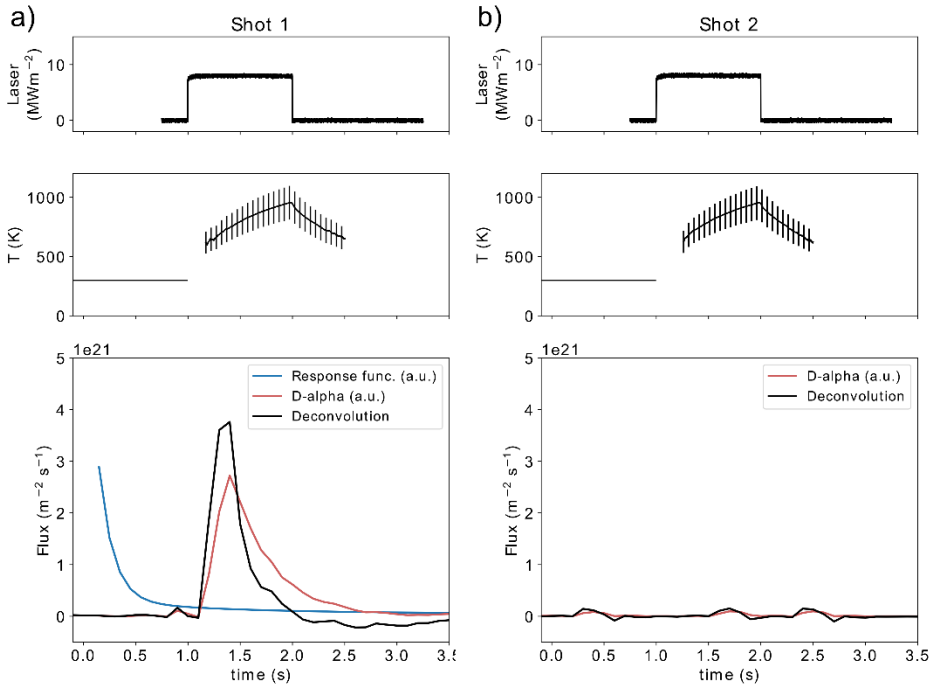

Figure 7 Two successive LIDS measurements with 1 s pulses on 1.2 µm thick W-D codeposit with sample diameter 6 mm and laser spot diameter 10 mm. Data shown: laser power pulse waveform (top), pyrometer surface temperature measurement (middle), and Dα emission (bottom) during LIDS (red), system response function measured offline after LIDS (blue), and the calibrated deconvolution of the response function and Dα (black). The inferred areal D retention is $1.3\pm0.4 \times 10^{21}$ m^{-2}, in excellent agreement with conventional TPD analysis, as shown in Figure 8.

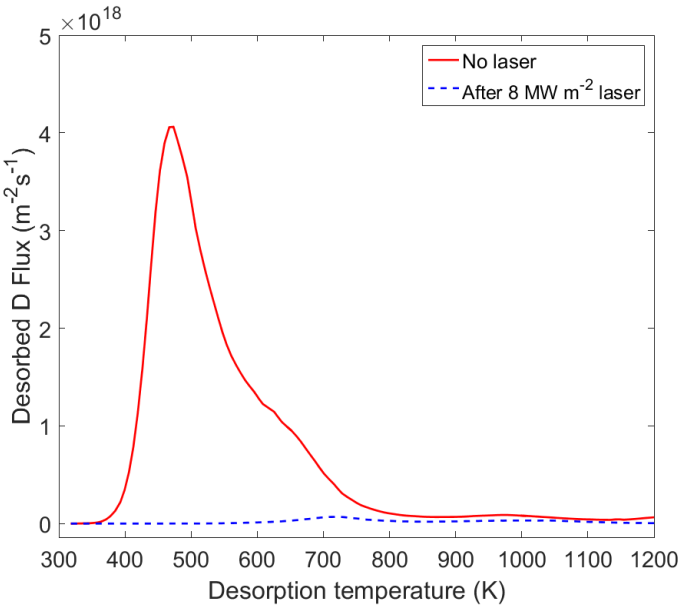

Figure 8 TPD using a temperature ramp rate of 0.3 Ks-1 for two W-D codeposits from the same deposition run (1.2 μm layer thickness with 330 K sample temperature), with no laser desorption (red), and after 1 s laser desorption (blue).

C. RF Power and Pressure Scan

Use of the D_2 calibration leak for each plasma condition where LIDS is performed provides a direct method to quantify each LIDS D release independent of the plasma properties. The rf power and argon fill pressure were varied in order to check this assumption, by investigating if changing plasma parameters would affect the LIDS measurement, if at all. Figure 9a shows the electron density and temperature, measured with a Langmuir probe located 28 cm above the sample, as a function of rf power. Two argon fill pressures of 1.8 and 10.6 mTorr were investigated, and the plasma density is seen to vary by a factor of ~1.8, while T_e was fairly constant. The LIDS retention measurements from W-D codeposits, shown in Figure 9b, were found to be relatively constant for all rf powers and Ar pressures, demonstrating, as expected, that the technique is robust to variations of these parameters, at least in the ranges explored.

A summary comparison of LIDS and TPD is shown in Figure 10, showing agreement over nearly four orders of magnitude in measured areal D retention. The largest source of error in the 25 mm diameter Ti-D samples was uncertainty on the area of desorption, while at low signals for the two W-D samples, the error was due to low signal-noise ratio. That is, low signal-to-noise limited the LIDS diagnostic in the present configuration to detection of a minimum of ~10^{20} Dm^{-2}, however, higher density plasmas will be used in future work which will allow increased sensitivity. For the W-D codeposits near 1.3×10^{21} m^{-2} with full laser coverage, excellent agreement is seen between the LIDS and TPD measurements.

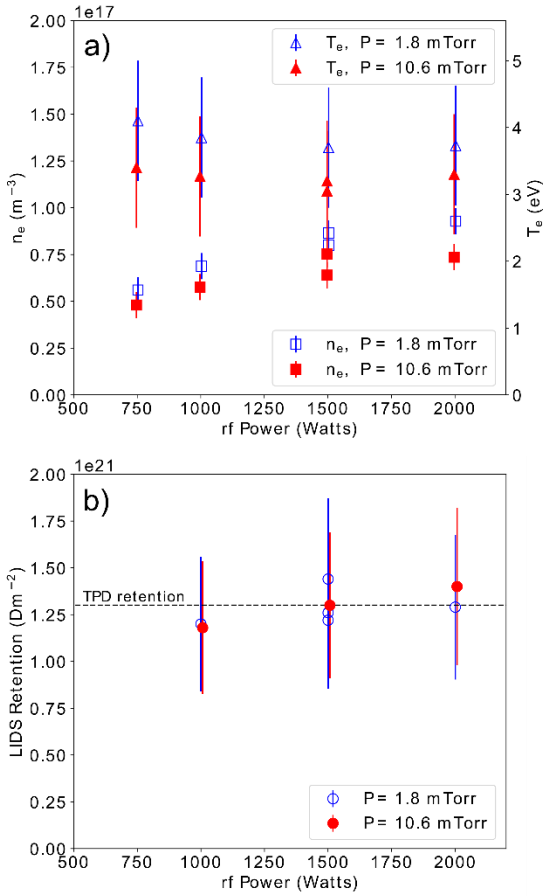

Figure 9 Scan of rf power showing a) electron density (squares) and temperature (triangles) for Ar fill pressures of 1.8 mTorr (blue) and 10.6 mTorr (red). b) LIDS retention measurements from 8 W-D codeposits all created from the same batch. Dashed line shows D retention of a sample from the same batch, measured using TPD.

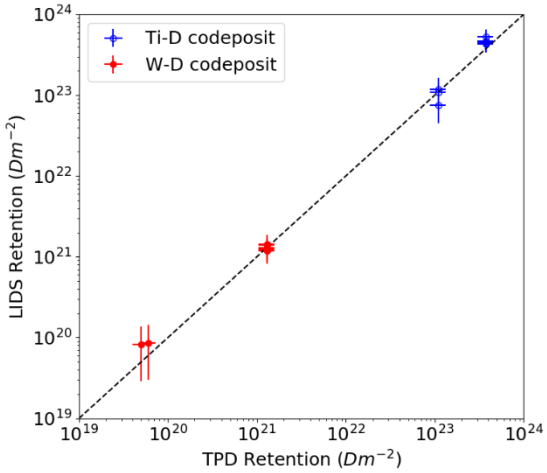

Figure 10 Deuterium retention measured using LIDS compared with TPD, where the dashed line indicates one-to-one agreement.

VI. Summary

We have presented methods and techniques to analyze laser-desorbed particle flux measured using optical spectroscopy in a background plasma, and applied those analysis methods to Ti-D and W-D codeposits in Ar plasma. The main contributions of this work are: 1) Separate measurements of Dα and Hα from separate D_2 and H_2 gas injections are obtained, which allows simultaneous determination of Dα and Hα during LIDS using spectral fitting, 2) A calibrated leak of D_2 is used to convert the spectroscopic signal to particle flow rate. This requires the leak source to be located near the laser-irradiated surface. When this condition is met, the calibration is robust because precise knowledge of the spatially-dependent plasma parameters along the spectroscopic line of sight is not needed, in contrast to the widely used S/XB method. More exotic, alternative methods of calibration could also be used in an actual fusion device, for example, a pellet filled with a known quantity of D_2 gas could be injected and then laser-ablated, providing a calibrated source of gas near the measurement location. 3) The system response function is measured experimentally using an impulsive burst of D_2 gas injection, and numerical deconvolution of the LIDS signal with the system response function provides a correction for time-dependent system effects such as wall recycling and finite pumping speed. Note that recycling cannot be properly removed from the measured signal using other popular signal processing techniques such as background subtraction. The use of deconvolution is not limited to optical spectroscopic measurements, and can, for example, be used for mass spectrometry or any other time-resolved measurement of desorbed species.

Acknowledgments

This work was supported by US DOE grant DE-SC0018281.

References

1. R.P. Doerner, G.R. Tynan, K. Schmid, Implications of PMI and wall material choice on fusion reactor tritium self-sufficiency, Nucl. Mater. Energy. 18 (2019) 56–61. doi:10.1016/J.NME.2018.12.006.

2. Report on Scientific Challenges and Research Opportunities in Plasma Materials Interactions (PMI), FES Workshop on Plasma Materials Interactions, http://science.energy.gov/~/media/fes/pdf/workshop-reports/2016/PMI_fullreport_21Aug2015.pdf.

3. V. Philipps et al., Nucl. Fusion 53 (2013) 093002.

4. A. Huber et al., Fusion Eng. Des. 86, 1336 (2011). doi.org/10.1016/j.fusengdes.2011.01.090

5. B. Schweer et al., Physica Scripta 2009 (2009) T138.

6. D. Nishijima, M. Patino, and R. P. Doerner, Rev. Sci. Instrum. 89, 10J105 (2018)

7. C. Grisolia et al., J. Nucl. Mater. 363-365, 1138 (2007). doi:10.1016/j.jnucmat.2007.01.169

8. C. Li, CL. Feng, H.Y. Oderji, et al., Front. Phys. 11, 114214 (2016). doi.org/10.1007/s11467-016-0606-1

9. Q. Xiao et al., J. Nucl. Mater. 463, 911 (2015).

10. L. Mercadier et al., J. Nucl. Mater. 415, S1187–90 (2011).

11. A. Semerok and C. Grisolia, Nucl. Instrum. Methods Phys. Res. A 720, 31 (2013).

12. K. Piip et al., J. Nucl. Mater. 636, 919 (2015).

13. P. Paris et al. Fusion Eng. Des. 98–99, 1349 (2015)

14. N. Gierse at al., Phys. Scr. T167, 014034 (2016).

15. D.D.R. Summers et al., J. Nucl. Mater. 290, 496 (2001).

16. B. Schweer et al., Journal of Nuclear Materials 390, 576 (2009).

17. M. Zlobinski et al., Phys. Scr. T145, 014027 (2011).

18. M. Zlobinski et al., Fusion Eng. Des. 86, 1332 (2011).

19. F. Schwirzke, H. Brinkschulte and M. Hashmi, J. Appl. Phys. 46 (1975) 4891.

20. B. L. Doyle and F. L. Vook, J. Nucl. Mater. 85&86, 1019 (1979).

21. C.H. Skinner et al., J. Nucl. Mater. 313-316, 496 (2003).

22. K. Hirata et al., Journal of Nuclear Materials 443, 298 (2013).

23. B. Schweer, F. Irrek, G. Sergienko, V. Philipps, U. Samm, J. Nucl. Mater. 363, 1375 (2007).

24. M. Zlobinski et al., Journal of Nuclear Materials 438, S1155 (2013).

25. J.H. Yu, M. Simmonds, M.J. Baldwin, R.P. Doerner, Nucl. Mater. and Energy 12, 749 (2017).

26. E.S. Marmar, J. Nucl. Mater. 76, 59 (1978).

27. M.J. Weber, Handbook of Optical Materials, Boca Raton, CRC Press (2003).

28. J.H. Yu, M.J. Baldwin and R.P. Doerner, Phys. Scripta 2017, T170 (2017).

29. J.H. Yu, G. De Temmerman, R.P. Doerner, R.A. Pitts, Nucl. Fusion. 55, 093027 (2015). doi:10.1088/0029-5515/55/9/093027

30. Y. Hirooka, J. Vac. Science and Technology A 2 (1984) 16

31. M.J. Simmonds, J.H. Yu, et al., J. Nucl. Mater 508 (2018) 472